Breaking Rayleigh's curse for two unbalanced single-photon emitters using BLESS technique

KONSTANTIN KATAMADZE[1,2,*], BORIS BANTYSH[1,3], ANDREY CHERNYAVSKIY[1,3], YURII BOGDANOV[1,3], AND SERGEI KULIK[2]

[1] *Valiev Institute of Physics and Technology, Russian Academy of Sciences, 117218, Moscow, Russia*
[2] *Quantum Technology Centre, Faculty of Physics, M. V. Lomonosov Moscow State University, 119991, Moscow, Russia*
[3] *Russian Quantum Center, Skolkovo, Moscow 143025, Russia*
[*] *k.g.katamadze@gmail.com*

Compiled November 9, 2023

According to the Rayleigh criterion, it is impossible to resolve two independent point sources separated by a distance below the width of the point spread function (PSF). Almost twenty years ago it was shown that the distance between two point sources can be statistically estimated with an accuracy better than the PSF width. However, the estimation error increases with decreasing distance. This effect was informally named Rayleigh's curse. Next, it was demonstrated that PSF shaping allows breaking the curse provided that all other source parameters except for the distance are known *a priori*. In this work, we propose a novel imaging technique based on the target Beam moduLation and the Examination of Shot Statistics (BLESS). We show that it is capable of breaking Rayleigh's curse even for unbalanced point sources with unknown centroid and brightness ratio. Moreover, we show that the estimation precision is close to the fundamental limit provided by the quantum Cramér–Rao bound.

http://dx.doi.org/10.1364/ao.XX.XXXXXX

1. INTRODUCTION

The standard diffraction theory claims that the far-field linear optical imaging resolution is restricted by the Rayleigh limit: two point sources cannot be resolved if the distance between them is smaller than the point spread function (PSF) width, which is proportional to the radiation wavelength [1]. There are many techniques allowing to overcome the Rayleigh limit [2]. Some of them are based on nonlinear light-matter interaction [3], complex systems of excitation and suppression of luminescence [4], and consequently have a very limited field of application.

A different strategy allowing super-resolved imaging is based on the usage of a prior information about the object. Describing the whole object with a few parameters reduces the imaging problem to the problem of statistical estimation. In particular, van den Bos group considered the problem of two point sources localization [5, 6]. Using the model of Gaussian PSF, they concluded that if the distance d between sources is larger than PSF width σ, its estimation error Δ_d is proportional to $\frac{\sigma}{\sqrt{K}}$, where K is the number of registered events. If $d < \sigma$ then $\Delta_d \propto \frac{\sigma}{\sqrt{Kd/\sigma}}$. Hence, the distance between two close point sources cannot be accurately estimated with a limited amount of data. This problem was named Rayleigh's curse [7].

Later Tsang et al showed the possibility to overcome Rayleigh's curse [7–9]. They considered the problem of resolving two equal point sources in terms of quantum Fisher information (QFI). They proved that QFI was independent of the distance d value, which means that the parameter can be precisely estimated beyond the Rayleigh limit. Moreover, the QFI limit can almost be saturated by practical measurement protocols: SPAtial-Mode DEmultiplexing (SPADE) [7] and SuperLocalization by Image inVERsion interferometry (SLIVER) [8]. Both protocols make use of the PSF (or detection/target mode) shaping. In particular, the use of odd PSF instead of even Gaussian PSF breaks Rayleigh's curse. This has been demonstrated in the set of proof-of-principle experiments [10–13].

But it was later shown that the Rayleigh's curse can be overcome for the two-parameter object model only [14–20]. Two unbalanced point sources with unknown brightness ratio [15, 17] or more than two equal sources [14] cannot be precisely localized beyond the Rayleigh limit: the position estimation error increases polynomially with decreasing distance between sources.

In general, any object can be parameterized by its intensity moments. It was shown that the estimation errors of the first and the second intensity moments are independent of the object size, but the Rayleigh's curse still holds for higher k-order moments M_k, resulting in $\Delta_{M_k} \propto d^{1-k/2}$, so they cannot be well estimated beyond the Rayleigh limit [18–20].

To perform precise imaging of complex objects one needs to extract additional information from measurements. Previ-

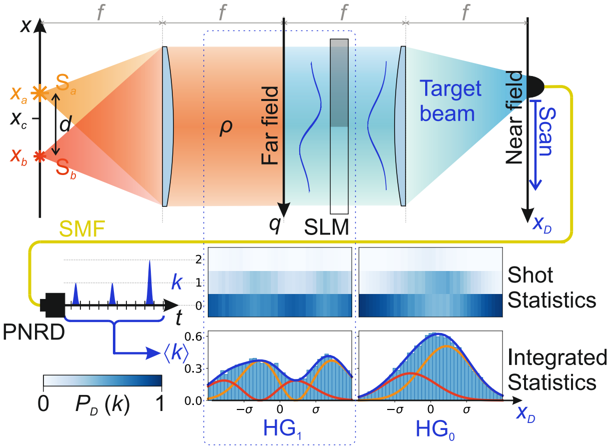

Fig. 1. The principal imaging scheme. SLM – spatial light modulator, SMF – single-mode fiber, PNRD – photon number resolving detector.

ously, most of the imaging statistical estimation problems were considered in the weak source approximation, where the number of detected photons was not greater than 1, and the spatial distribution of mean photon number was measured [7–20].

However, higher order intensity (or photon number) moments give benefits for solving imaging problems. One of the first demonstrations of this was done by Brown and Twiss in their stellar interferometer experiment [21]. It was later shown that PSF for N-order intensity moment measurement was $\sqrt{N}$ times narrower than the first-order one [22]. This was experimentally applied to the single-photon emitters imaging [23–27]. Also, intensity fluctuation analysis was used for single molecule localisation (SML) techniques like STochastic Optical Reconstruction Microscopy (STORM) [28] and PhotoActivated Localization Microscopy (PALM) [29] techniques, where the positions of independently blinking point sources were estimated from a set of frames obtained at different times. Initially, these techniques required that only one molecule emitted within a PSF area at any given time. However, advanced methods [22, 30, 31] employ intensity correlation analysis to relax this stringent requirement. Traditional SML techniques [22, 28–31] rely on long-term ($> \mu$s) intensity fluctuations associated with blinking and bleaching phenomena. Short-term photon correlations ($< \mu$s), on the other hand, have primarily been utilized for efficient PSF narrowing purposes [23–27]. Recently, there has been a shift towards applying photon statistics analysis to address the localization problem in point sources with varying photon statistics [32–34]. However, breaking Rayleigh's curse through this approach has not yet been reported.

Below in Section 2 we propose an approach that combines the statistical estimation of image parameters, PSF shaping and the examination of photon statistics distribution. We consider the localization of single-photon sources as an example, particularly prevalent in fluorescence microscopy, where one need to resolve individual molecules of fluorophores employed in staining biological tissues [35]. In Section 3 we describe the motivation behind using this approach. Using the classical and quantum Cramér–Rao bound (Section 4) we show that this technique allows breaking Rayleigh's curse for two unbalanced single-photon emitters (Section 5).

2. BLESS TECHNIQUE

Consider a 1D imaging problem for two uncorrelated single-photon point sources S_a and S_b located at x_a and x_b respectively (Fig. 1). The sources have the following photon number distributions:

$$P_{a,b}(n) = \delta_{0n}(1-\mu_{a,b}) + \delta_{1n}\mu_{a,b}, \tag{1}$$

where δ_{ij} is the Kronecker delta, μ_a and μ_b are mean photon numbers. One can describe this object using the following set of 4 parameters:

- distance $d = x_a - x_b$,
- total mean photon number $\mu = \mu_a + \mu_b$,
- centroid $x_c = (\mu_a x_a + \mu_b x_b)/\mu$,
- relative brightness $\gamma = (\mu_a - \mu_b)/\mu \in [-1, 1]$.

The light from the source is passed throw a $4f$ imaging system with 1:1 magnification. Since the imaging lens has a limited numerical aperture (NA), the light from the source s, located at x_a has a Gaussian far-field electric field

$$\tilde{\Psi}_a(q) = \frac{1}{(\pi\sigma^2)^{1/4}} \exp\left[-\frac{q^2\sigma^2}{2} + \mathrm{i}x_a\right], \tag{2}$$

which is related to the Gaussian near-field electric field

$$\Psi_a(x) = \frac{1}{(\pi\sigma^2)^{1/4}} \exp\left[-\frac{(x-x_a)^2}{2\sigma^2}\right], \tag{3}$$

called Point Spread Function (PSF). Its width $\sigma \sim \lambda/\mathrm{NA}$. For the source, located at x_b we have the similar equation for $\Psi_b(x)$.

In the image plane light is coupled to the single-mode fiber (SMF) collimator which forms a Gaussian target (detection) mode at position x_D with waist σ_0:

$$\Psi_0(x) = \frac{1}{(\pi\sigma_0^2)^{1/4}} \exp\left[-\frac{(x-x_D)^2}{2\sigma_0^2}\right]. \tag{4}$$

Here and below lower index D corresponds to the detection process. Scanning x_D one can measure the image profile. Additionally, one can place a Spatial Light Modulator (SLM) between the lenses which transforms the Gaussian HG_0 Target Mode into the first Hermite-Gaussian mode HG_1 with the field distribution

$$\Psi_1(x) = \frac{\sqrt{2}(x-x_D)}{\sigma_0(\pi\sigma_0^2)^{1/4}} \exp\left[-\frac{(x-x_D)^2}{2\sigma_0^2}\right]. \tag{5}$$

Bellow we will show that this target beam modulation combined with a photon number distribution measurement plays a key role in precise emitters localization.

In order to measure the photon number distribution, the SMF output is connected to a photon number resolving detector (PNRD). For simplicity we assume the detector quantum efficiency to be 100%. The probability of detecting a single photon emitted by the point source S_a is then

$$T_a^{(0,1)} = \left|\int \Psi_{0,1}^*(x)\Psi_a(x)\mathrm{d}x\right|^2. \tag{6}$$

Here and bellow we consider the case $\sigma_0 = \sigma$ which is a tradeoff between the high resolution and high efficiency. Under this condition

$$T_a^{(0)} = \exp\left[-\frac{(x_a-x_D)^2}{2\sigma^2}\right] \tag{7}$$

for HG_0 Target Mode and

$$T_a^{(1)} = \frac{(x_a - x_D)^2}{2\sigma^2} \exp\left[-\frac{(x_a - x_D)^2}{2\sigma^2}\right] \quad (8)$$

for HG_1 Target Mode.

Then the total probability of detecting k photons from the source S_a is

$$P_{a,D}(k|\boldsymbol{\theta}, x_D) = \sum_{n=k}^{\infty} \binom{n}{k} P_a(n) T_a^k (1 - T_a)^{n-k}. \quad (9)$$

The probability distribution $P_{b,D}$ for the source S_b is calculated in the similar way.

Since the sources are uncorrelated, the convolution of $P_{a,D}$ and $P_{b,D}$ gives the detected photon number distribution, which depends on the detector position x_D and image parameters $\boldsymbol{\theta} = \{d, \gamma, \mu, x_c\}$:

$$\begin{aligned} P_D(k|\boldsymbol{\theta}, x_D) = & \delta_{0k}(1 - M_a)(1 - M_b) + \\ & \delta_{1k}(M_a + M_b - 2M_a M_b) + \\ & \delta_{2k} M_a M_b, \end{aligned} \quad (10)$$

where $M_a = \mu_a T_a$, $M_b = \mu_b T_b$. The mean detected photon number for this distribution is

$$M_D(x_D) = M_a + M_b, \quad (11)$$

the variance is

$$\sigma_D^2(x_D) = M_a(1 - M_a) + M_b(1 - M_b), \quad (12)$$

and the normalized second-order correlation function is

$$g_D^{(2)}(x_D) = \frac{2M_a M_b}{(M_a + M_b)^2}. \quad (13)$$

The process of the statistical reconstruction of image parameters is performed through the measurement of photocounts across detector positions. The acquisition time is divided into the intervals comparable to the emitters' lifetimes (shots). This division enables to measure photocount histograms reflecting the detected photon number distribution. The object parameters are then derived by fitting function P_D with parameters $\boldsymbol{\theta}$ to histograms. This innovative approach makes use of both the target Beam moduLation and the Examination of Shot Statistics (BLESS), effectively enabling us to achieve subdiffraction emitter localization.

Meanwhile, the standard approach exploits the integrated number of registered photons: one estimates the parameters from measuring Eq. (11) only.

Experimentally, the use of integrated statistics corresponds to a single measurement with a long exposition time, while the shot statistics analysis assumes many measurements with a short exposition time.

3. WHY BLESS?

To understand how the target mode shaping and photon statistics measurements can improve the two point resolution, consider the example presented in Fig. 2. The object consists of two point sources S_a and S_b with coordinates $x_a = \sigma/\sqrt{2}$, $x_b = -\sigma/\sqrt{2}$ and mean emitted photon numbers $\mu_a = 0.1$, $\mu_b = 0.2$. Usual imaging scheme allows one to measure the mean photon number M_D versus the detector position x_D (we assume the Gaussian PSF of the detector with the width σ). This

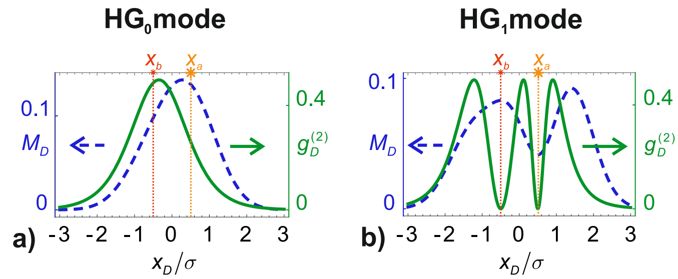

Fig. 2. The detected mean photon number M_D (blue dashed lines) and the second-order correlation function $g_D^{(2)}$ (green solid lines) vs. detector position x_D in units of σ for the Gaussian HG_0 PSF (left) and for the Hermite-Gaussian HG_1 PSF (right). The object consists of two point sources S_a and S_b with coordinates $x_a = \sigma/\sqrt{2}$, $x_b = -\sigma/\sqrt{2}$ and mean generated photon numbers $\mu_a = 0.1$, $\mu_b = 0.2$.

dependence is presented by the blue dashed line on the left plot. This image looks like a single Gaussian function, which center is shifted to the left, since the left source is brighter, and it is really hard to resolve two sources from this picture. If one transforms the Target Mode to the Hermite-Gaussian mode HG_1 and again measures the mean photon number, they obtain an image, presented by the blue dashed line on the right plot. Here we can see the two peaks and a dip between them. Its depth depends both on the distance d between two sources and on their relative brightness γ, so if one of these parameters is known *a priory*, it is easy to estimate another one from this plot, but if both parameters are unknown, it is still difficult to estimate them. However, one can measure the photon number distribution at each position x_D and calculate the second-order correlation function Eq. (13) which is presented as a green solid line on both plots. Both $g_D^{(2)}$ plots differ from M_D plots and they can carry some additional information about the object parameters. For the HG_1 Target Mode case the improvement is really huge and quite visible. If the detector position x_D exactly equals the position x_a, it register no light from the source S_a since HG_1 function is asymmetrical and gives zero overlap with the Gaussian PSF Eq. (8). So, in this point detector register the light from the only one single-photon source S_b and therefore the $g_D^{(2)}$ function exactly equals zero at this point. By the same reason $g_D^{(2)}$ has a minimum at $x_D = x_b$. This means that correlation function has narrow dips at the positions of single-photon sources, which can be used for their precise localization.

This approach can be generalized to a large number of independent single-photon sources N since even in this case $g_D^{(N)}$ correlation function has narrow minima at the sources locations. Therefore, the photon number distribution measurement (which contain information about all the correlation functions) combined with the asymmetric shaping of the target mode, can provide the subdiffraction photon source localization.

4. LIMITS ON PARAMETERS ESTIMATION

A. Cramér–Rao bound (CRB)

Consider a *statistically efficient unbiased* estimate $\hat{\boldsymbol{\theta}}$ of four image parameters. For each imaging experiment, $\hat{\boldsymbol{\theta}}$ is a random vector having multivariate normal distribution $f(\hat{\boldsymbol{\theta}})$ centered at point $\boldsymbol{\theta}^*$ of the true parameters values [36, 37]. According to CRB, the covariance matrix Σ of $f(\hat{\boldsymbol{\theta}})$ is the inverse of the 4×4 Fisher information matrix I with elements

$$I_{\alpha\beta} = \sum_k \frac{[\partial_\alpha \mathcal{P}(k)][\partial_\beta \mathcal{P}(k)]}{\mathcal{P}(k)}\bigg|_{\boldsymbol{\theta}=\boldsymbol{\theta}^*}, \quad \textbf{(14)}$$

where $\mathcal{P}$ is the detector photon number distribution Eq. (10), and ∂_α is its partial derivative with respect to the parameter θ_α [36, 37]. The values $\Delta_\alpha = \sqrt{[I^{-1}]_{\alpha\alpha}}$ thus describes the statistical limits of the parameters θ_α estimation error. Since the Fisher information is additive over independent trials, we define the complete information matrix as $I = \sum_{x_D} K_{x_D} I_{x_D}$. Here we take the sum over various target beam positions x_D with the corresponding sample size K_{x_D} and Fisher information matrix I_{x_D}.

Non-efficient estimators give $\Sigma > I^{-1}$ ($\Sigma - I^{-1}$ is a positive-definite matrix). The bound $\Sigma = I^{-1}$ is usually attainable for the maximum-likelihood estimator (see **Supplement 1**, section 1) but the maximization routine becomes slower with decreasing distance d. Moreover, we expect the computation complexity to increase tremendously with the increasing amount of light sources and consequently the number of parameters to estimate. In this regard, it is important to discover efficient methods for solving this optimization problem.

For the integrated statistics we analyze the information carried by the mean photon number M_D in each detector position x_D. The Fisher information for estimating M_D is just K_{x_D}/σ_D^2, so the information matrix for object parameters is

$$I^M_{\alpha\beta} = \frac{K_{x_D}}{\sigma_D^2(x_D)}[\partial_\alpha M_D(x_D)][\partial_\beta M_D(x_D)]. \quad \textbf{(15)}$$

As before, summing up over different x_D gives the complete information matrix. Note that considering the integrated statistics is similar to the widely used weak source approximation [7–20]. Below we will demonstrate that it does not provide enough information in order to break Rayleigh's curse for unbalanced point sources.

B. Quantum CRB

Fisher information matrix depends on the particular measurements. However, one might be interested in the ultimate limit over all possible measurements. This could be achieved by computing the quantum Fisher information matrix [7, 14, 38]:

$$I^Q_{\alpha\beta} = 2\sum_{kl,\lambda_k+\lambda_l\neq 0} \frac{\langle\psi_k|\partial_\alpha\rho|\psi_l\rangle\,\langle\psi_l|\partial_\beta\rho|\psi_k\rangle}{\lambda_k+\lambda_l}\bigg|_{\boldsymbol{\theta}=\boldsymbol{\theta}^*}. \quad \textbf{(16)}$$

Here ρ is the image density matrix, $\rho = \sum_j \lambda_j \left|\psi_j\right\rangle\!\left\langle\psi_j\right|$ – its spectral decomposition. The quantum CRB is then the inverse of matrix I^Q.

Following the proposed BLESS approach one defines the density matrix ρ of the light in the image plane taking into account both photon number and spatial degrees of freedom. For two single-photon sources one obtains

$$\rho = w_0 \left|0\right\rangle\!\left\langle 0\right| + w_{1_a}\left|1_a\right\rangle\!\left\langle 1_a\right| + w_{1_b}\left|1_b\right\rangle\!\left\langle 1_b\right| + w_2\left|2\right\rangle\!\left\langle 2\right|. \quad \textbf{(17)}$$

Here $w_0 = P_a(0)P_b(0)$ is the probability of vacuum state (0 photons), $w_{1_a} = P_a(1)P_b(0)$ ($w_{1_b} = P_a(0)P_b(1)$) is the probability of the source A (B) to emit a single photon, $w_2 = P_a(1)P_b(1)$ is the probability to get 2 photons from both sources. The corresponding states are

$$\begin{aligned} \left|1_a\right\rangle &= q_a^\dagger\left|0\right\rangle, \quad \left|1_b\right\rangle = q_b^\dagger\left|0\right\rangle, \\ \left|2\right\rangle &= \frac{q_a^\dagger q_b^\dagger}{\sqrt{1+V^2}}\left|0\right\rangle, \end{aligned} \quad \textbf{(18)}$$

where

$$q^\dagger_{a,b} = \int \Psi_{a,b}(x)a^\dagger(x)dx \quad \textbf{(19)}$$

are the creation operators for Gaussian modes, $a^\dagger(x)$ is the creation operator for coordinate x, $\Psi_a(x)$ and $\Psi_b(x)$ are Gaussian functions, centered at x_a and x_b respectively (see eq. Eq. (3)). The overlap integral between two modes is

$$V \equiv \int \Psi_a(x)\Psi_b^*(x)dx = \exp\left(-\frac{d^2}{4\sigma^2}\right). \quad \textbf{(20)}$$

The computation of Eq. (16) is a bit tricky since operators $q_a^\dagger$ and $q_b^\dagger$ are not orthogonal (do not commute). We first introduce a set of eight non-orthogonal states that supports Eq. (17) and its derivatives. Then we perform its numerical orthogonalization. The resulting orthonormal basis is used to get the matrix representation of the operators in Eq. (16) and compute the quantum Fisher information matrix. See details in **Supplement 1**, section 2.

5. RESULTS AND DISCUSSION

We have analyzed lower bounds for the estimation accuracy of source parameters depending on the distance d between two unbalanced point sources and their brightness ratio γ. Fig. 3 shows the estimation errors (standard deviations) for parameters d (a, c, e), γ (b, d, f), μ (g) and x_c (h). Note that we multiply all Δ_α by $\sqrt{K}$ ($K = \sum_{x_D} K_{x_D}$) to make them sample size independent. The plots for $\Delta\mu$ and Δx_c almost don't depend on the value of γ, so we present them for $\gamma = 0.1$ only, but $\Delta_d(d)$ and $\Delta_\gamma(d)$ dependencies are significantly different for distinct γ. Below we discuss the main observations from the plots.

A. Distance d estimation error

The quantum CRB for the distance error $\Delta_d^{(Q)}$ does not depend on d for all the gamma values, which means that the Rayleigh's curse can be overcome. We have empirically found the following simple relation:

$$\Delta_d^{(Q)} = \frac{\sqrt{2}\sigma}{\sqrt{\mu-\mu^2/2}\sqrt{1-\gamma^2}\sqrt{K}}. \quad \textbf{(21)}$$

This dependency on γ means that d can be estimated better for the sources with similar brightness than for significantly unbalanced sources. The dependency of μ means that for small mean photon number most of the shots have no photons and so do not carry any information about the source.

For classical CRB the errors look different for different measurement protocols. For two equal point sources with $\gamma = 0$ (Fig. 3a) the photon number statistics examination give no benefit: both solid lines (blue and red) and both dashed lines are perfectly matched. However, the target mode transformation significantly helps. For HG_0 target mode $\Delta_d \propto d^{-1}$, which corresponds to the Rayleigh's curse, presented in [5, 6]. At the same time, for HG_1 mode Rayleigh's curse is dispelled: Δ_d saturates at $d/\sigma \sim 0.1$ and then remains constant for $d < 0.1\sigma$ as well as it was presented in [7–9].

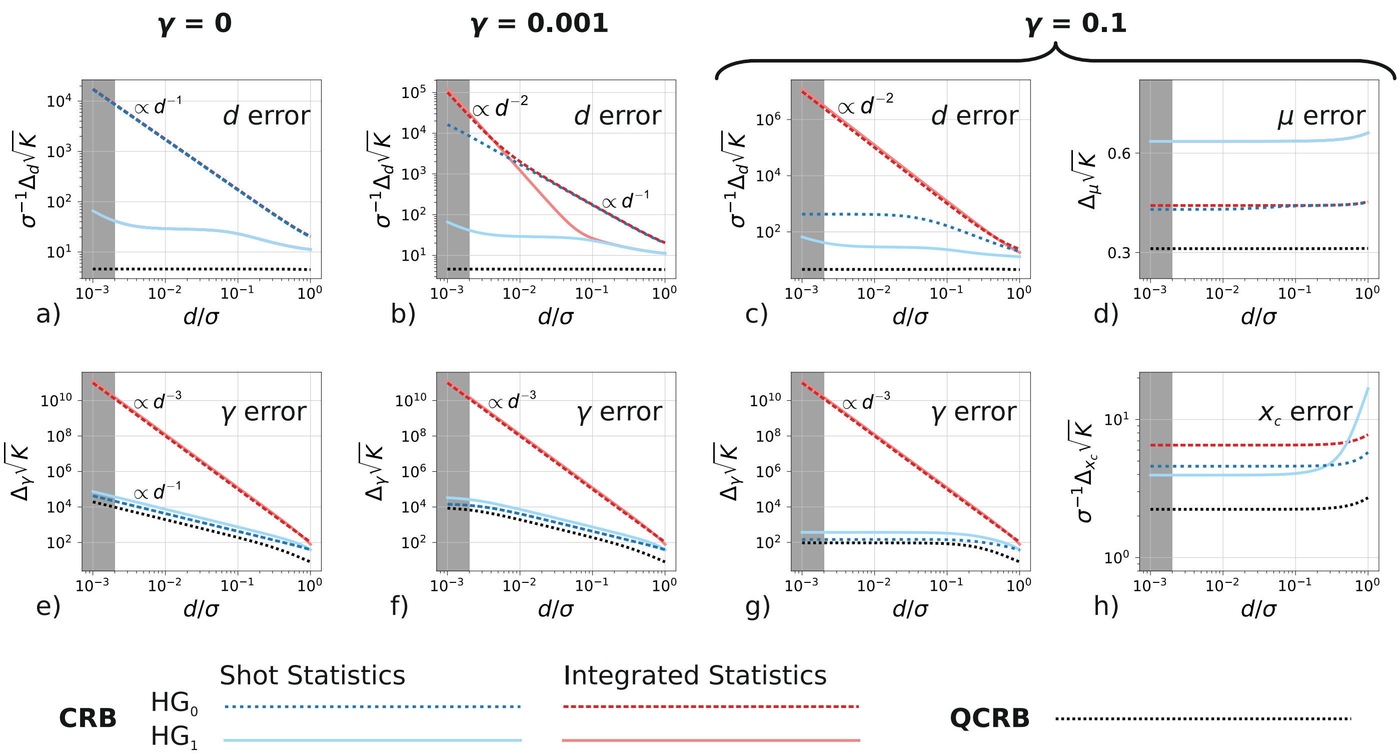

Fig. 3. Normalized estimation errors of the distance between the point sources d (a, b, c), their relative brightness γ (e, f, g), total mean photon number μ (d) and centroid x_c (h) versus d. The total mean photon number $\mu = 0.1$. The relative brightness $\gamma = 0$ (a, e), $\gamma = 0.001$ (b, f), $\gamma = 0.1$ (c, d, g, h). Black dotted line corresponds to the quantum Cramér–Rao bound, other lines – to classical Cramér–Rao bounds with different measurement protocols: dashed lines correspond to Gaussian PSF, solid lines – to HG_1-mode PSF, red lines correspond to the mean photon number measurements, blue lines – to the shot statistics analysis. For all the protocols detector position $x_D/\sigma = -2, -1.9, \ldots, 1.9, 2$ and the centroid position $x_c/\sigma = 0.001$. The proposed BLESS technique corresponds to HG_1-mode PSF and the shot statistics analysis (blue solid line). Note that the mesh x_D does not contain the unknown centroid location x_c, and the error for BLESS technique starts to grow when $d \lesssim 2x_c$ (gray regions on the plots).

Here and bellow, $\Delta_d(d)$ remains constant while there is a node in the detector position mesh in between two sources positions (i.e. $x_a > x_D > x_b$ for some x_D). It means that for high resolution one needs to decrease the scanning step or adjust the detector position adaptively. If this condition is not satisfied, the estimation error Δ_d starts to grow, which we can see in Fig. 3(a–c) for the blue solid line in the range $d/\sigma \lesssim 2 \times 10^{-3} = x_c/\sigma$, selected with gray.

For unbalanced point sources with $\gamma = 0.1$ (Fig. 3c) and higher, the $\Delta_d(d)$ dependencies are different. Measuring just a mean value in each image point can not give a precise estimation accuracy of the distance: for both HG_0 and HG_1 target modes $\Delta_d \propto d^{-2}$, which matches the results presented in [17]. However, shot statistics examination allows to limit Δ_d. For HG_0 mode $\Delta_d\sqrt{K} \sim 10^3$ for $d/\sigma < 10^{-2}$ and for HG_1 mode $\Delta_d\sqrt{K} \sim 10$ for $d/\sigma < 10^{-1}$. So, for this case the target beam modulation can increase the accuracy by two orders of magnitude, but does not qualitatively change the $\Delta_d(d)$ dependency.

Note, that in [17] quantum CRB leads to $\Delta_d \propto d^{-1}$ for unbalanced sources, but for our model, considering photon-number distribution, quantum CRB leads to $\Delta_d = const$, which means, that full model allows better results even from the fundamental point of view.

In the intermediate case with $\gamma = 0.001$ (Fig. 3b), one can see that the combination of the target beam modulation and the shot statistics examination allows limitation of $\Delta_d(d)$ dependency (beating the Rayleigh's curse), while all the other measurement protocols demonstrate an error growth as $\Delta_d \propto d^{-1}$ and $\Delta_d \propto d^{-2}$.

Therefore, for all the values of γ BLESS protocol limits the $\Delta_d(d)$ dependency which is qualitatively close to quantum CRB $\Delta_d = const$, but for $d \to 0$ the quantum CRB value is ~ 10 times lower than the best considered classical CRB. It means, that our measurement protocol is still not optimal and can be improved. For example, parallel image acquisition in all the image pixels instead of point-by-point scanning can significantly boost the measurements, but it requires much more complicated equipment.

B. Brightness ratio γ estimation error

As one can see from (Fig. 3e–g), the brightness ratio estimation error Δ_γ almost does not depend on the choice of the target mode (dashed and solid lines stay very close). Independently on the γ value integrated statistics measurement leads to $\Delta_\gamma \propto d^{-3}$. Shot statistics examination allows better precision. For balanced sources with $\gamma = 0$ (Fig. 3e) it leads to $\Delta_\gamma \propto d^{-1}$ and for unbalanced sources with $\gamma = 0.1$ (Fig. 3g) Δ_γ saturates to the constant level for $d/\sigma < 0.1$ for shot statistics examination. For the intermediate case with $\gamma = 0.001$ (Fig. 3f) the error dependency $\Delta_\gamma(d)$ also saturates, but at higher level and for smaller values of d. For all the plots presented in Fig. 3(e–g) one can note that quantum CRB curve is close to the classical CRB for shot examination protocols, but a bit lower.

C. Integral parameters μ and x_c estimation errors

The integral source parameters μ and x_c (Fig. 3d, h) can be well-estimated with all the measurement protocols. For $d < 0.1\sigma$ all CRB for all the protocols as well as quantum CRB lead to $\Delta_\mu(d) = const$ and $\Delta_{x_c}(d) = const$. However for the centroid x_c BLESS allow higher accuracy than other protocols.

The increase of x_c estimation error for high values of d (which takes place for all the CRB plots) can be explained with two reasons. First, for higher values of d larger part of the image is not covered by the mesh $x_D/\sigma = -2, -1.9, \ldots, 1.9, 2$. Second, it can be shown that for $d \gg \sigma$ the error $\Delta_{x_c} \propto d$. By definition

$$x_c \equiv \frac{\mu_a x_a + \mu_b x_b}{\mu_a + \mu_b}. \quad (22)$$

For well-separated sources all the parameters x_a, x_b, μ_a, and μ_b can be independently estimated with the corresponding errors. The error of the x_c value can be calculated as an indirect measurement error:

$$\Delta^2_{x_c} = \frac{d^2(\mu_a^2\Delta^2_{\mu_b} + \mu_b^2\Delta^2_{\mu_a}) + \mu^2(\mu_a^2\Delta^2_{x_a} + \mu_b^2\Delta^2_{x_b})}{\mu^4}, \quad (23)$$

so, indeed for large d values $\Delta^2_{x_c} \propto d^2$.

D. Applicability of BLESS approach

Since our technique requires less prior information about the studying object (in comparison with all the previous methods beating the Rayleigh's curse [7–9]), it can be used for a wider range of real metrological applications. This includes improving both lateral [10–13] and axial [39, 40] resolution in microscopy, as well as elevating temporal [41] and spectral [42] resolution capabilities.

However, BLESS approach is limited by the localization of single-photon emitters, so its main application can be found in Single Molecule Localization (SML) field aimed to localize dye molecules attached to the biological samples [35]. Typical molecule size ~ 10 nm is about 10 times smaller than the confocal microscope PSF width $\sigma \sim 200 - 300$ nm. As follows from Eq. (21), for $\mu \sim 10^{-2}$ (which fits with an order of total emitter, detector, and imaging system efficiency) one needs to acquire about $K \sim 10^6$ shots to obtain 10 times resolution enhancement $(\Delta_d \sim \sigma/10)$. According to Fig. 3e, the distance error Δ_d for BLESS can be 10 times bigger than quantum CRB, so real number of shots can reach $K \sim 10^8$. However, the shot duration should be about a dye molecule lifetime $\tau \sim$ ns, therefore the total acquisition time is less than 1 second, which is suitable for many imaging applications. In contrast with other SML techniques like STED [4], STORM/PALM [28, 29], BLESS technique does not require switchable dyes, so it can be used for a wider range of biological samples.

E. Research prospects

Our study is the first step in a comprehensive research program. This program includes a study of the scalability of BLESS with an increase in the number of emitters [14, 43] and an assessment of its robustness against experimental imperfections such as background illumination, detector noise, etc [44–46]. Moreover, our approach can be extended to point sources with different photon statistics, including thermal sources and partially coherent sources [41, 47–49]. The use of adaptive measurement strategies [50], and machine-learning approach for optimization of the measurement protocol[51] and fast photon statistics analysis[27] can also be promising.

6. CONCLUSION

In conclusion, we have proposed a novel imaging technique. This technique is based on the multi-shot photon number measurements in the modulated target beam that scans the object. Image parameters are then estimated by fitting the photon number distribution model to the collected data. The approach has been theoretically studied on the example of two unbalanced single-photon sources. The Cramér–Rao bound (both classical and quantum) analysis has shown that even for infinitely close sources the estimation error of the distance between them is limited. Thus, we have demonstrated that the form of photon number distribution should be used in the statistical estimation of image parameters since it provides an additional information, and in particular allows one to break Rayleigh's curse. The proposed method can be used for the single molecule localization and other microscopy applications.

Funding. This research was performed according to the MSU Program of Development, Project No 23-SCH06-05, and supported by the State Program no. FFNN-2022-0016 for Valiev Institute of Physics and Technology of RAS, and by the Russian Foundation for Basic Research (project no. 20-32-70153).

Acknowledgments. We acknowledge useful discussions with Stanislav Straupe, Egor Kovlakov, Tatiana Smirnova, Stephen Vintskevich and René Reimann.

Disclosures. The authors declare no conflicts of interest.

Data availability. Data underlying the results presented in this paper are not publicly available at this time but may be obtained from the authors upon reasonable request.

Supplemental document. See **Supplement 1** for supporting content.

REFERENCES

1. F. R. S. Rayleigh, "Xxxi. investigations in optics, with special reference to the spectroscope," The London, Edinburgh, Dublin Philos. Mag. J. Sci. **8**, 261–274 (1879).
2. P. R. Hemmer and T. Zapata, "The universal scaling laws that determine the achievable resolution in different schemes for super-resolution imaging," J. Opt. **14**, 083002 (2012).
3. J. Squier and M. Muller, "High resolution nonlinear microscopy: A review of sources and methods for achieving optimal imaging," Rev. Sci. Instrum. **72**, 2855 (2001).
4. T. Müller, C. Schumann, and A. Kraegeloh, "Sted microscopy and its applications: New insights into cellular processes on the nanoscale," ChemPhysChem **13**, 1986–2000 (2012).
5. S. Van Aert, A. den Dekker, D. Van Dyck, and A. van den Bos, "High-resolution electron microscopy and electron tomography: resolution versus precision," J. Struct. Biol. **138**, 21–33 (2002).
6. E. Bettens, D. Van Dyck, A. den Dekker, *et al.*, "Model-based two-object resolution from observations having counting statistics," Ultramicroscopy **77**, 37–48 (1999).
7. M. Tsang, R. Nair, and X.-M. Lu, "Quantum theory of superresolution for two incoherent optical point sources," Phys. Rev. X **6**, 031033 (2016).
8. R. Nair and M. Tsang, "Interferometric superlocalization of two incoherent optical point sources," Opt. Express **24**, 3684 (2016).
9. R. Nair and M. Tsang, "Far-field superresolution of thermal electromagnetic sources at the quantum limit," Phys. Rev. Lett. **117**, 190801 (2016).
10. P. Boucher, C. Fabre, G. Labroille, and N. Treps, "Spatial optical mode demultiplexing as a practical tool for optimal transverse distance estimation," Optica **7**, 1621 (2020).
11. M. Paúr, B. Stoklasa, J. Grover, *et al.*, "Tempering rayleigh's curse with psf shaping," Optica **5**, 1177 (2018).

12. M. Paúr, B. Stoklasa, Z. Hradil, *et al.*, “Achieving the ultimate optical resolution,” Optica **3**, 1144 (2016).
13. W.-K. Tham, H. Ferretti, and A. M. Steinberg, “Beating rayleigh’s curse by imaging using phase information,” Phys. Rev. Lett. **118**, 070801 (2017).
14. E. Bisketzi, D. Branford, and A. Datta, “Quantum limits of localisation microscopy,” New J. Phys. **21**, 123032 (2019).
15. K. A. G. Bonsma-Fisher, W.-K. Tham, H. Ferretti, and A. M. Steinberg, “Realistic sub-rayleigh imaging with phase-sensitive measurements,” New J. Phys. **21**, 093010 (2019).
16. L. Peng and X. M. Lu, “Generalization of rayleigh’s criterion on parameter estimation with incoherent sources,” Phys. Rev. A **103**, 1–10 (2021).
17. J. Řehaček, Z. Hradil, B. Stoklasa, *et al.*, “Multiparameter quantum metrology of incoherent point sources: Towards realistic superresolution,” Phys. Rev. A **96**, 062107 (2017).
18. M. Tsang, “Subdiffraction incoherent optical imaging via spatial-mode demultiplexing: Semiclassical treatment,” Phys. Rev. A **97**, 023830 (2018).
19. M. Tsang, “Quantum limit to subdiffraction incoherent optical imaging,” Phys. Rev. A **99**, 1–12 (2019).
20. S. Zhou and L. Jiang, “Modern description of rayleigh’s criterion,” Phys. Rev. A **99**, 1–20 (2019).
21. R. Hanbury Brown and R. Q. Twiss, “A test of a new type of stellar interferometer on sirius,” Nature **178**, 1046–1048 (1956).
22. T. Dertinger, R. Colyer, G. Iyer, *et al.*, “Fast, background-free, 3d super-resolution optical fluctuation imaging (sofi),” Proc. National Acad. Sci. **106**, 22287–22292 (2009).
23. D. Gatto Monticone, K. Katamadze, P. Traina, *et al.*, “Beating the abbe diffraction limit in confocal microscopy via nonclassical photon statistics,” Phys. Rev. Lett. **113**, 143602 (2014).
24. O. Schwartz and D. Oron, “Improved resolution in fluorescence microscopy using quantum correlations,” Phys. Rev. A **85**, 33812 (2012).
25. O. Schwartz, J. M. Levitt, R. Tenne, *et al.*, “Superresolution microscopy with quantum emitters.” Nano Lett. **13**, 5832–5836 (2013).
26. R. A. Bartels, G. Murray, J. Field, and J. Squier, “Super-Resolution Imaging by Computationally Fusing Quantum and Classical Optical Information,” Intell. Comput. **2022**, 1–11 (2022).
27. Z. A. Kudyshev, D. Sychev, Z. Martin, *et al.*, “Machine learning assisted quantum super-resolution microscopy,” Nat. Commun. **14**, 4828 (2023).
28. M. J. Rust, M. Bates, and X. Zhuang, “Sub-diffraction-limit imaging by stochastic optical reconstruction microscopy (storm),” Nat. Methods **3**, 793–796 (2006).
29. E. Betzig, G. H. Patterson, R. Sougrat, *et al.*, “Imaging intracellular fluorescent proteins at nanometer resolution,” Science **313**, 1642–1645 (2006).
30. N. Gustafsson, S. Culley, G. Ashdown, *et al.*, “Fast live-cell conventional fluorophore nanoscopy with ImageJ through super-resolution radial fluctuations,” Nat. Commun. **7**, 12471 (2016).
31. E. Nehme, L. E. Weiss, T. Michaeli, and Y. Shechtman, “Deep-STORM: super-resolution single-molecule microscopy by deep learning,” Optica **5**, 458 (2018).
32. A. B. Mikhalychev, B. Bessire, I. L. Karuseichyk, *et al.*, “Efficiently reconstructing compound objects by quantum imaging with higher-order correlation functions,” Commun. Phys. **2**, 134 (2019).
33. Y. Wang, Y. Zhang, and V. O. Lorenz, “Superresolution in interferometric imaging of strong thermal sources,” Phys. Rev. A **104**, 022613 (2021).
34. N. Bhusal, M. Hong, A. Miller, *et al.*, “Smart quantum statistical imaging beyond the Abbe-Rayleigh criterion,” npj Quantum Inf. **8**, 83 (2022).
35. M. Lelek, M. T. Gyparaki, G. Beliu, *et al.*, “Single-molecule localization microscopy,” Nat. Rev. Methods Primers **1**, 39 (2021).
36. H. Cramér, *Mathematical Methods of Statistics* (Princeton University Press, 1999).
37. M. G. Kendall and A. Stuart, *The Advanced Theory of Statistics, Vol. 2: Inference and Relationship* (Charles Griffin and Company Ltd., 1961).
38. J. Liu, H. Yuan, X.-M. Lu, and X. Wang, “Quantum fisher information matrix and multiparameter estimation,” J. Phys. A: Math. Theor. **53**, 023001 (2020).
39. D. Koutný, Z. Hradil, J. Řeháček, and L. L. Sánchez-Soto, “Axial super-localization with vortex beams,” Quantum Sci. Technol. **6** (2021).
40. Y. Zhou, J. Yang, J. D. Hassett, *et al.*, “Quantum-limited estimation of the axial separation of two incoherent point sources,” Optica **6**, 534 (2019).
41. S. De, J. Gil-Lopez, B. Brecht, *et al.*, “Effects of coherence on temporal resolution,” Phys. Rev. Res. **3**, 033082 (2021).
42. M. Paúr, B. Stoklasa, D. Koutný, *et al.*, “Reading out fisher information from the zeros of the point spread function,” Opt. Lett. **44**, 3114 (2019).
43. C. Lupo, Z. Huang, and P. Kok, “Quantum limits to incoherent imaging are achieved by linear interferometry,” Phys. Rev. Lett. **124**, 80503 (2020).
44. C. Lupo, “Subwavelength quantum imaging with noisy detectors,” Phys. Rev. A **101**, 22323 (2020).
45. G. Sorelli, M. Gessner, M. Walschaers, and N. Treps, “Optimal observables and estimators for practical superresolution imaging,” Phys. Rev. Lett. **127**, 123604 (2021).
46. G. Sorelli, M. Gessner, M. Walschaers, and N. Treps, “Moment-based superresolution: Formalism and applications,” Phys. Rev. A **104**, 033515 (2021).
47. S. Kurdzialek, “Back to sources – the role of coherence in super-resolution imaging revisited,” arXiv: 2103.12096v1 (2021).
48. M. Tsang and R. Nair, “Resurgence of rayleigh’s curse in the presence of partial coherence: comment,” Optica **6**, 400 (2019).
49. S. A. Wadood, K. Liang, Y. Zhou, *et al.*, “Experimental demonstration of superresolution of partially coherent light sources using parity sorting,” Opt. Express **29**, 22034 (2021).
50. E. F. Matlin and L. J. Zipp, “Adaptive imaging of arbitrary thermal source distributions with near quantum-limited resolution,” ArXiV 2106.13332 (2021).
51. A. Durand, T. Wiesner, M.-A. Gardner, *et al.*, “A machine learning approach for online automated optimization of super-resolution optical microscopy,” Nat. Commun. **9**, 5247 (2018).